Superplasticity of liquid-Phase Sintered β-SiC

Takayuki Nagano

Abstract

The compression and the tension tests of liquid-phase sintered β-SiC fabricated by hot-pressing using ultra fine powders were performed at 1973 K ~ 2048 K in N_2 atmosphere. Amorphous phases were observed at the grain boundaries and at multi-grain junctions in the as-sintered material. Strain hardening was observed under all experimental conditions. Stress exponents in the compression test were from 1.7 to 2.1 in the temperature ranging from 1973 K to 2023 K. A maximum tensile elongation of 170 % was achieved at the initial strain rate of 2 X 10^{-5} s^{-1} at 2048 K.

1. Introduction

Superplasticity is phenomenologically defined as an ability of polycrystalline material to exhibit an extraordinary large elongation (> 100 %) during the tension test. Ceramics superplasticity was discovered in ionic 3 mol% Y_2O_3-stabilized tetragonal zirconia polycrystals (3Y-TZP) in 1985 [1]. Ceramics superplasticity is generally exhibited on the polycrystals with the average grain size less than 1 μm. However, in the solid phase sintering of SiC with the additions of B and C, it was difficult to obtain submicron-sized SiC because of covalent nature of Si-C bonding and low self-diffusion coefficient. Therefore, superplasticity of SiC (140 %) was discovered in B, C-doped β-SiC with the grain size of 0.2 μm fabricated by ultra high pressure hot isostatic press (UHP-HIP) using the glass capsule in 1998 [2].

However, UHP-HIP process using glass capsule is a difficult route to get complex-shaped components and large volume bulk material. Besides, UHP-HIP process is too

expensive to apply for the practical use.

Liquid-phase sintering is an effective way to lower the sintering temperature and obtain the fine-grained material. Actually, SiC with the grain size about 0.2 μm could be obtained by liquid-phase sintering [3]. The presence of liquid phase at the grain boundaries promotes the deformation, and contributes the accommodation of stress concentration at the triple points. Authors investigated the high temperature deformation of liquid-phase sintered β-SiC with the additions of oxide additives and obtained about 60 % tensile elongation in Ar [4-6]. The fine initial grain size, low grain growth rate, and stability at elevated temperature are especially important for superplastic deformation. However, the tensile elongation of liquid-phase sintered β-SiC with the additions of oxide additives was prevented by the vaporization of liquid phase and the decomposition of SiC [6].

Authors also investigated the weight loss of liquid-phase sintered β-SiC with oxide additives during the heat treatment, and found that the weight loss in N_2 was suppressed abount 1/2 to 1/3 in comparison with the weight loss in Ar [7]. Although we performed the tension test of liquid-phase sintered β-SiC with oxide additives in N_2, maximum tensile elongation reached only about 11 % due to the crystallization of grain-boundary phase [8].

It was reported that the microstructure of SiC with the addition of oxynitride glass was stable at elevated temperatures in N_2, and grain growth and phase transformation were suppressed [9-10]. Accordingly, the deformation of liquid-phase sintered SiC with oxynitride glass in N_2 is thought to cause the suppression of grain growth, the phase transformation, the vaporization of liquid phase and the decomposition of SiC. Moreover, the viscosity of liquid phase with nitrogen is high, and the occurrence of cavitation should be suppressed.

Therefore, we investigated the deformation behavior of liquid-phase sintered β-SiC with

the addition of oxynitride glass at elevated temperature in N_2.

2. Experimental procedure

2.1 Specimen preparation

Starting material was ultra fine β-SiC powder (T-1 grade, Sumitomo-Osaka Cement Co., Tokyo, Japan) fabricated by chemical vapor deposition (CVD) method. It was oxidized at 873 K for 1 h in air to eliminate free carbon and hydrofluoric acid-treated to remove SiO_2. The particle size was ~ 90 nm as calculated from the specific surface area. A mixture of 55.8 wt% Al_2O_3 (99.9 % pure, Sumitomo Chemical Co., Tokyo, Japan), 36.9 wt% Y_2O_3 (99.9 % pure, Shin-Etsu Chemical Co., Tokyo, Japan), and 7.3 wt% AlN (F Grade, Tokuyuma Soda Co., Tokyo, Japan) was prepared to an oxynitride composition by SiC ball milling in n-hexane. SiC was then mixed with 9 wt% oxynitride powder by SiC ball milling in n-hexane. The mixed powder was hot-pressed at 2073 K for 15 min under a stress of 30 MPa in N_2, and its bulk density was 3.21 g/cm^3.

As-sintered body was cut by diamond cutter and ground by diamond wheel. The size of compressive specimen was 2 X 2 X 3 mm. The specimen surfaces were mirror-polished with diamond pastes. Tensile specimen was dog-bone shape, having rectangular cross section (1 X 0.8 mm) with the gauge length of 4.4 mm. The gauge portion of tensile specimen was also mirror-polished with diamond paste.

2.2 Compression and tension test

Compression test and tension test at constant crosshead speeds were performed by using the universal testing machine at the initial strain rates from 1 X 10^{-4} s^{-1} to 5 X 10^{-6} s^{-1} at the temperature ranging from 1973 to 2048 K in N_2. The degree of specimen deformation was

evaluated from the displacement of crosshead. Compressive and tensile direction was perpendicular to the hot-pressing direction.

True strain (ε_t) is defined as

$$\varepsilon_t = \ln (l/l_0) \quad (1)$$

where l and l_0 are deformed and original gauge length, respectively.

By assuming homogeneous deformation process, true stress (σ_t) can be calculated by the following relation:

$$\sigma_t = P/A_0 \exp (\varepsilon_t) \quad (2)$$

where P is the applied load and A_0 is the cross section of the original specimen.

2.3 Microstructural observation

The specimens before and after the deformation were observed using the scanning electron microscopy (SEM: JSM-6330F, JEOL, Tokyo, Japan) on the polished and plasma etched surface with CF_4 + O_2 (8%) gas. The average grain size is defined by a linear intercept length as follows:

$$d_{av} = 1.776L \quad (3)$$

where d_{av} is the average grain size and L is the linear intercept length. X-ray analysis was also conducted (RINT2500, Rigaku, Tokyo, Japan). The polytypes of SiC were calculated by Tanaka's method [11]. Specimen was cut perpendicular to the compressive axis and prepared by the polishing and the argon-ion-beam thinning for transmission electron microscopy (TEM)

observation. High-resolution transmission electron microscopy (HRTEM) observation was performed by 200 kV TEM (JEM-2010MD, JEOL, Tokyo, Japan) and whose point-to-point resolution was 0.18 nm. The grain-boundary composition was analyzed by both electron energy loss spectroscopy (EELS) and energy dispersive X-ray spectroscopy (EDX). The energy loss spectroscopy was performed using an electron energy loss spectrometer attached to a scanning transmission electron microscope (HB601UX, VG, East Grinstead, U.K.), having a minimum probe size of 0.22 nm.

3. Result

3.1 Mechanical behavior

3.1.1 Compression test

The true stress-true strain curves at 1973 K are shown in Fig. 1. Crack was not observed from compressed specimens. Strain hardening was observed in all experimental conditions. Flow stress increased with increasing strain rate.

The strain rate ($\dot{\varepsilon}$) at the elevated temperature can be expressed as follows: [12)]

$$\dot{\varepsilon} = A\ \sigma^n/d^p \exp(-Q/RT) \qquad (4)$$

where A is a constant, σ the stress, d the grain size, Q the apparent activation energy, R the gas constant, n the stress exponent, and P the exponent of the inverse grain size.

The relationship between flow stress and strain rate is shown in Fig. 2. Stress exponents were calculated from the slope of lines. Stress exponents were from 1.7 to 2.1 in the temperature ranging from 1973K to 2023 K.

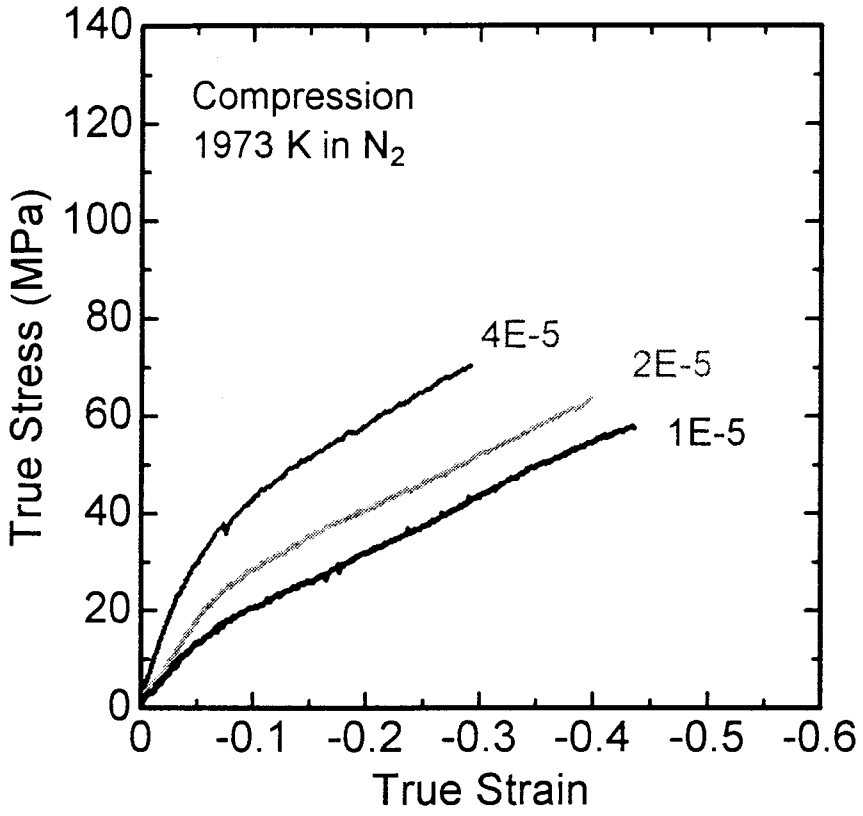

Fig. 1 True stress-true strain curves at 1973 K in N_2.

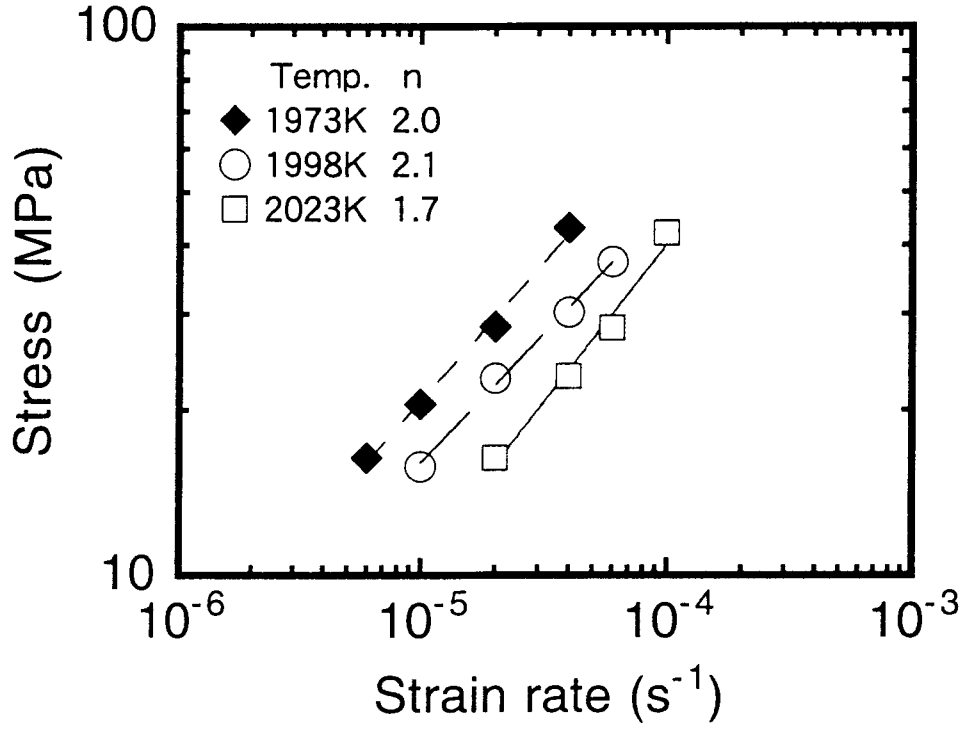

Fig. 2 Relationship between flow stress and strain rate.

The temperature dependence of strain rate is shown in Fig. 3. The apparent activation energy was 776 kJ/mol. This value is lower than that of lattice diffusion of Si and C (912 ± 5 kJ/mol, 814 ± 14 kJ/mol) and higher than that of grain-boundary diffusion of C (569 ± 9 kJ/mol) in high purity CVD β-SiC [13-14].

3.1.2 Tension test

The true stress-true strain curves at 2048 K are shown in Fig. 4. Strain hardening was observed in all experimental conditions. Flow stress was higher at lower strain rate in the beginning of deformation. Flow stress at the initial strain rate of 4 X 10^{-5} s^{-1} increased linearly with strain and fractured about 70 % elongation. Strain softening was observed before fracture at the initial strain rates of 1 X 10^{-5} s^{-1} and 2 X 10^{-5} s^{-1}. Tensile elongation of 170 % was achieved at the initial strain rate of 2 X 10^{-5} s^{-1}.

3.2 Microstructural change

3.2.1 Grain boundary structure

High-resolution TEM image of grain boundary of as-sintered material is shown in Fig. 5. An amorphous phase about 2 nm thickness was clearly observed at the grain boundary.

EELS results of as-sintered material are shown in Figs. 6 and 7. The peaks of Al, O and N which were not detected in SiC grain at the grain boundary. Moreover, the peak of Y was observed at grain boundary in EDX result. Therefore, this amorphous phase is thought to have the structure of Al_2O_3-SiO_2 glass with Y and N.

3.2.2 Dynamic change

Microstructural changes before and after compression and tension tests are shown in Fig. 8. As-sintered material was composed of equiaxed fine grains. An amorphous phase existed at the grain boundaries. In the deformed specimens, the anisotropy of grain growth

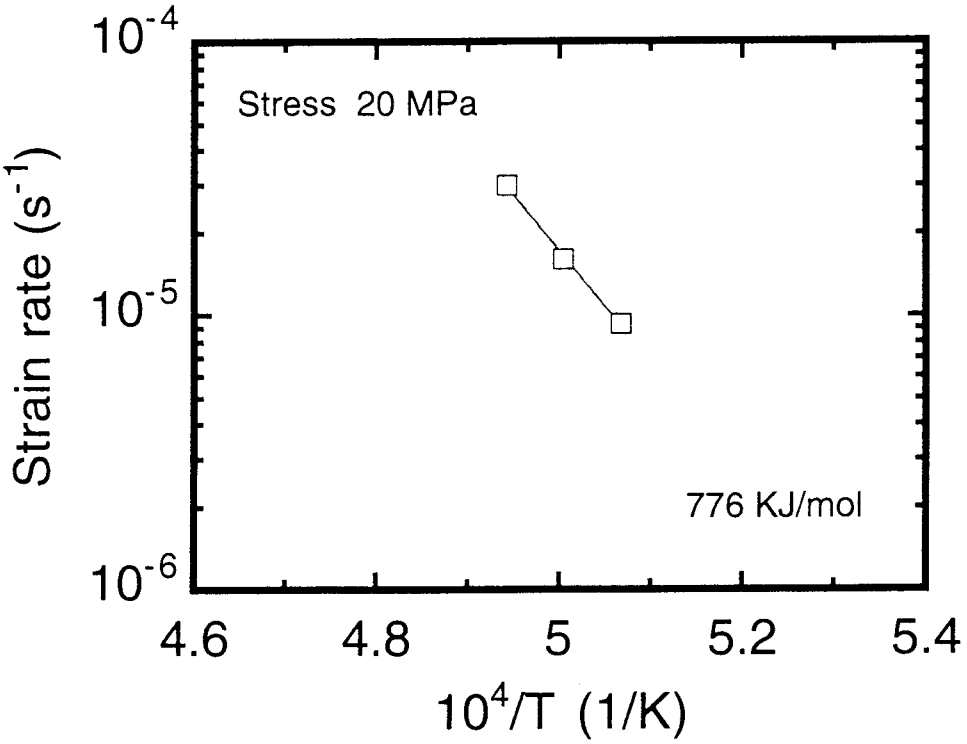

Fig. 3 Temperature dependence of strain rate.

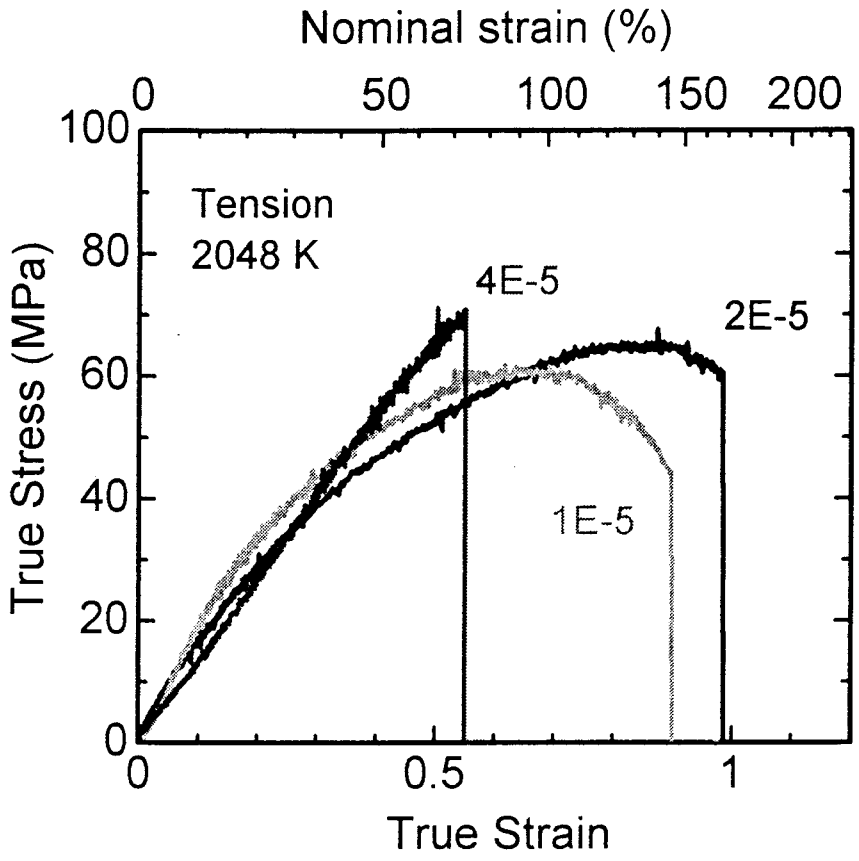

Fig. 4 True stress-true strain curves at 2048 K in N_2.

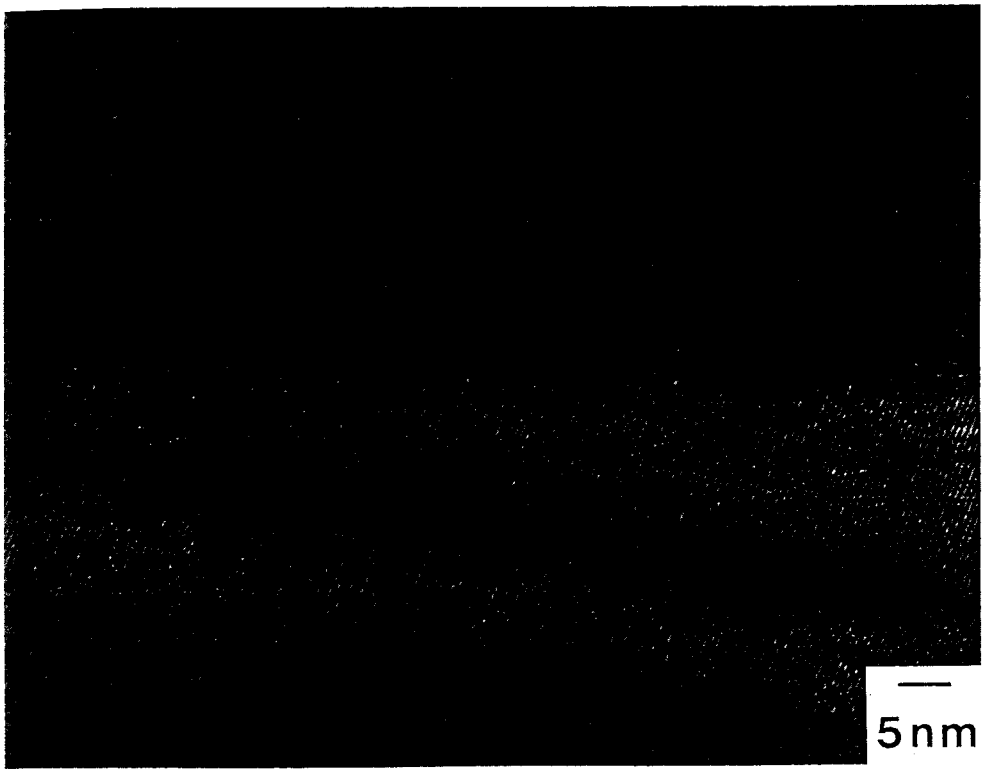

Fig. 5 High-resolution TEM image at grain boundary in as-sintered material.

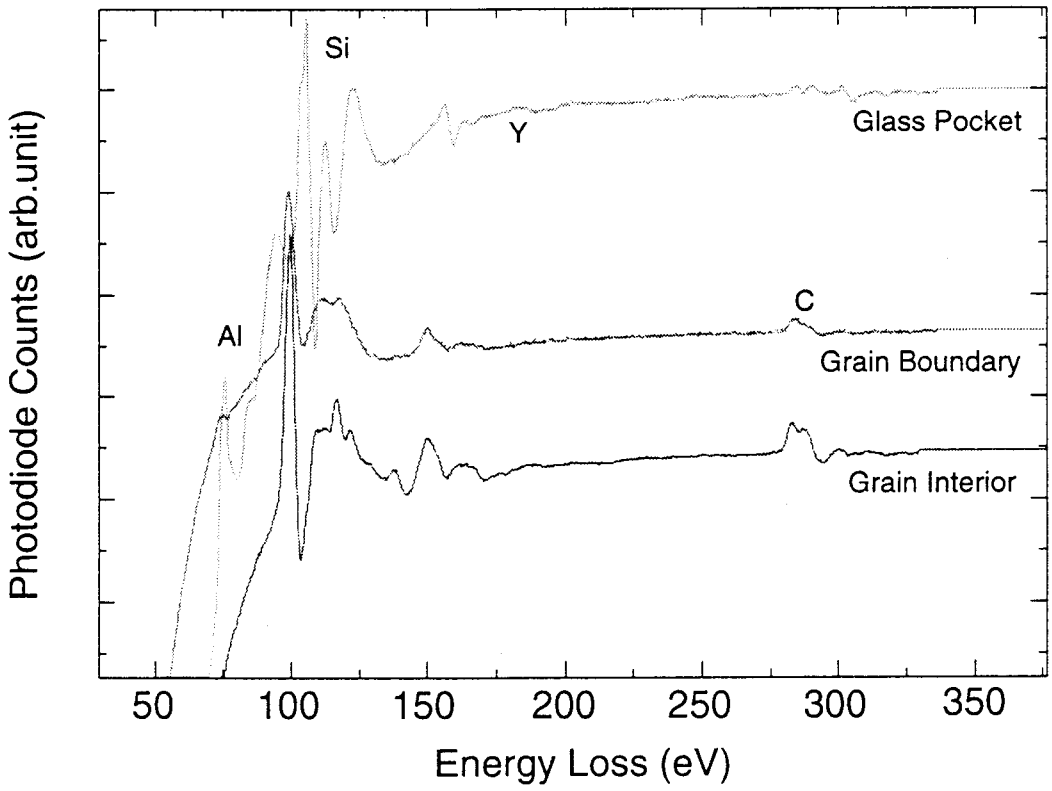

Fig. 6 EELS results for as-sintered material.

was observed and grains were elongated in the perpendicular direction of the compression axis. The aspect ratio was about 0.82 in the direction of compressive axis. Directly bonded grain boundaries increased after deformation.

On the other hand, almost amorphous phase was vaporized after the tensile deformation. Most of residual amorphous phase existed at the triple points. The anisotropy of grain growth was observed and grains were elongated in the direction of tensile axis. The grain aspect ratio was 1.44 in the direction of tensile axis.

Intergranular strain (ε_g) is defined as follows:

$$\varepsilon_g = \ln (d_{//}/d_{\perp}^{\,2} \cdot d_{//})^{1/3}$$

$$= 2/3 \ln (d_{//}/d_{\perp}) \qquad (5)$$

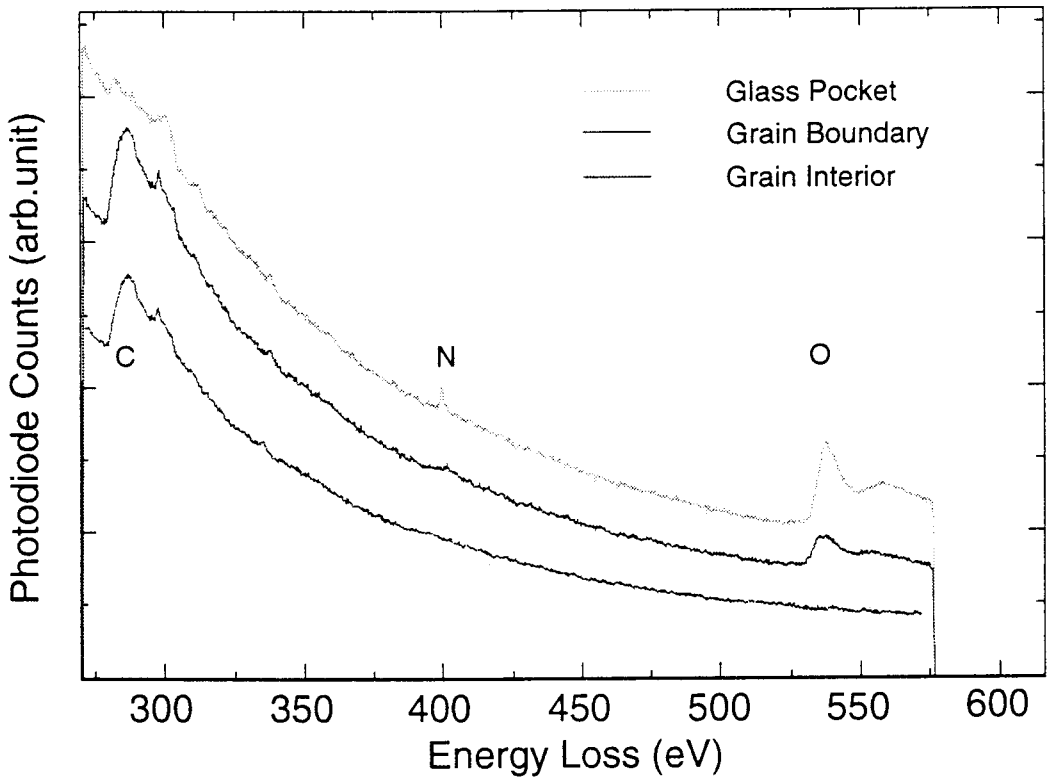

Fig. 7 EELS results for as-sintered material.

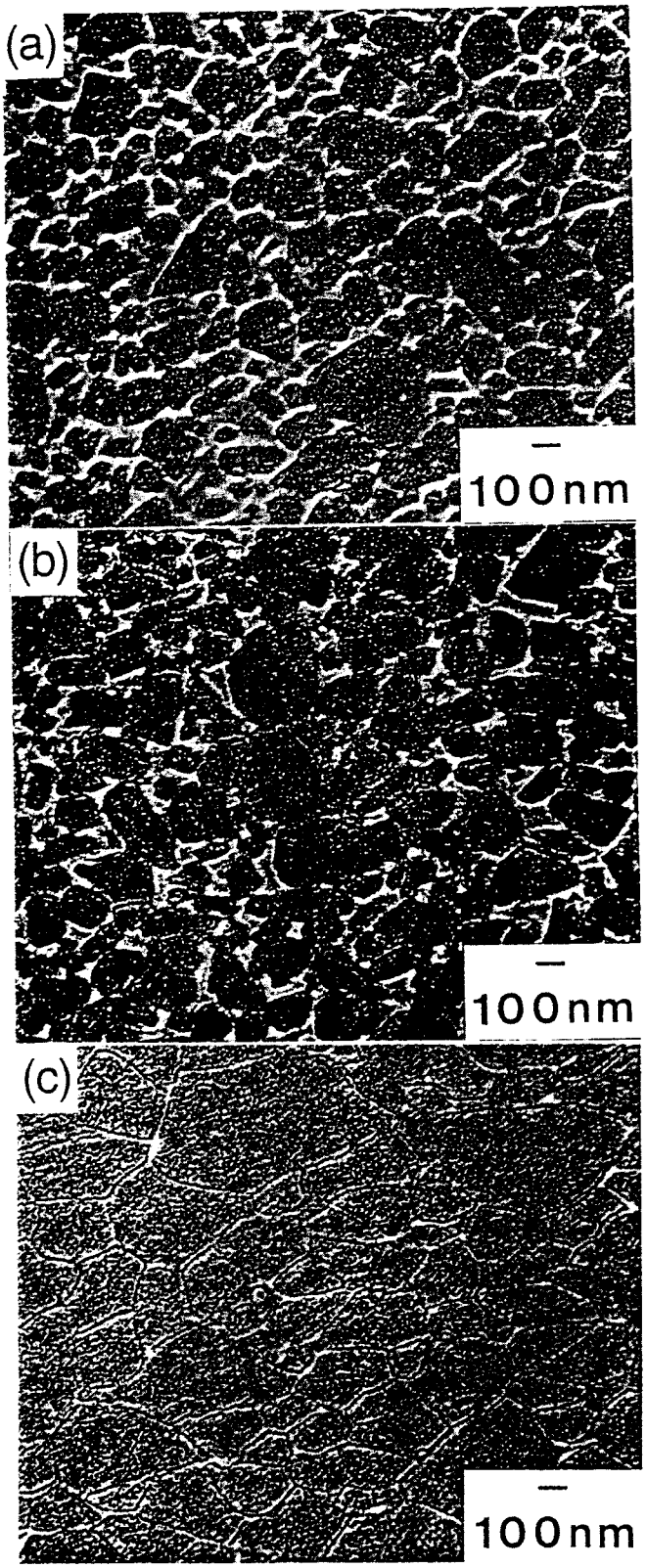

Fig. 8 Microstructure of (a) as-sintered SiC, (b) after compressive deformation (1998 K, $6X10^{-5}$ s^{-1}, 33 % strain, compressive axis is vertical), (c) after tensile deformation (2023 K, $1X10^{-5}$ s^{-1}, 153 % elongation, tensile axis is horizontal).

where $d_{//}$ is the grain size parallel to the tensile axis and $d_{\perp}$ is the grain size perpendicular to the tensile axis. The ratio of intergranular strain to the total strain (ε_{total}) is calculated to be about 24 %. If we assume that the total strain is the sum of intergranular strain and the strain by grain-boundary sliding, the strain caused by grain-boundary sliding is roughly estimated to be 76 %.

Grain size after the tensile deformation was about 7 times larger than that before the tension test in comparison with the size of short axis. The cavitation damage at gauge portion was almost suppressed even after 153 % tensile elongation.

TEM images of grain boundaries and grains after compressive deformation are shown in Figs. 9 and 10. An amorphous phase was not crystallized even after the compressive deformation. The dislocation which was thought to be formed by stress concentration at the triple point was slightly observed in SiC grains.

3.3 XRD analysis

The results of XRD analysis before and after the deformation are shown in Fig. 11. Crystalline phase of as–sintered material was almost β-SiC(3C) single phase. In compressed and tensiled specimens, the phase of α-SiC(6H) was observed. The contents of α-SiC for the compressed specimen and the tensiled specimen were calculated about 1 and 20 %, respectively. The specimen annealed for the testing time corresponded to 153 % tensile deformation at 2023 K in N_2 was also prepared to investigate the effect of strain for phase transformation from β to α. As the result, the content of α-SiC(6H) was about 15 % in annealed specimen.

4. Discussion

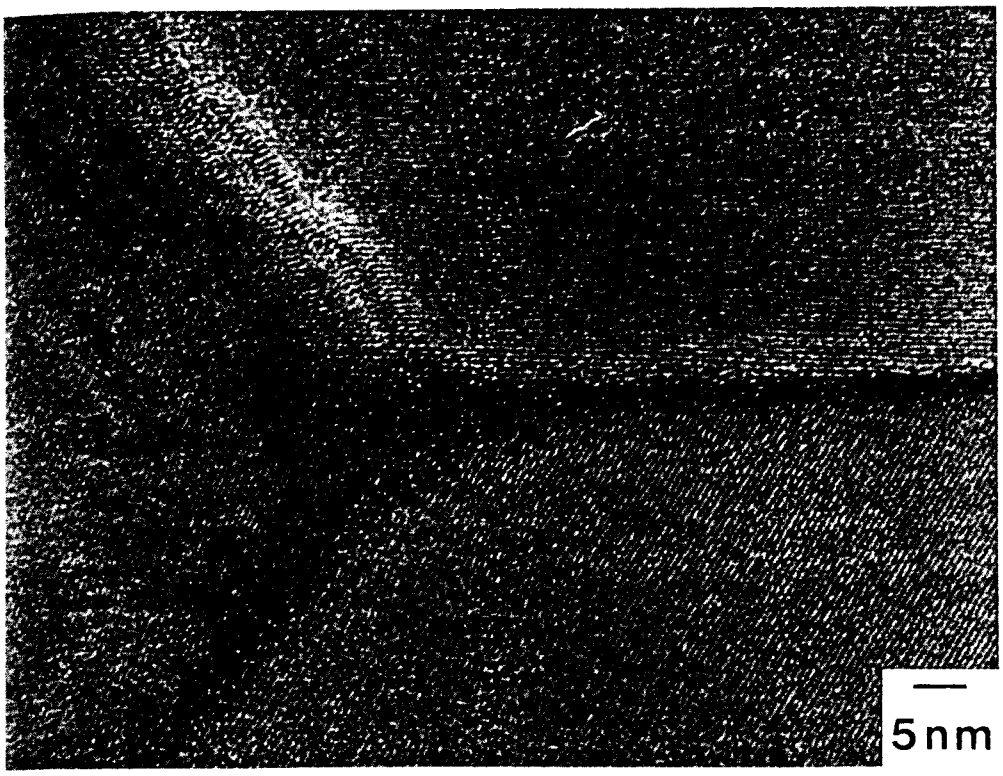

Fig. 9 High-resolution TEM image at grain boundaries after compressive deformation (1998 K, $4X10^{-5}$ s^{-1}, 35 % strain).

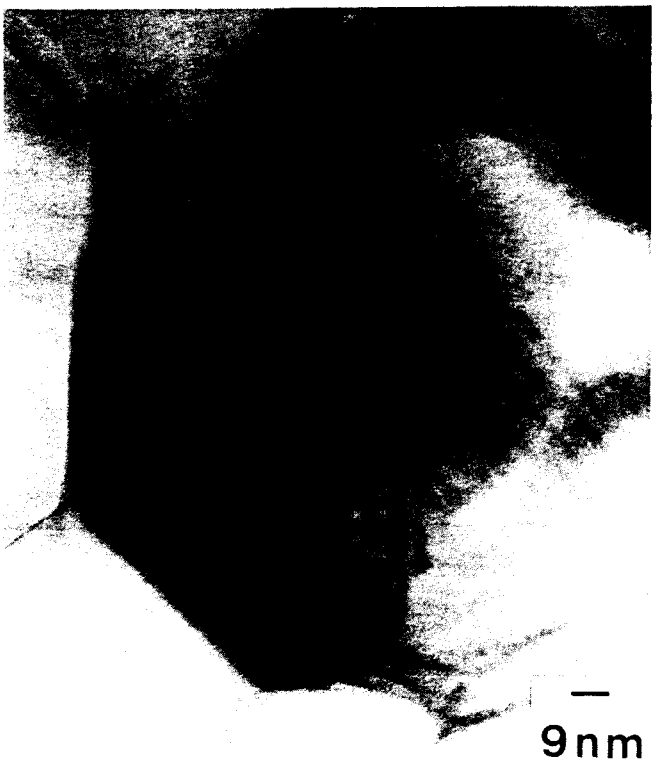

Fig. 10 TEM image after compressive deformation (1998 K, $4X10^{-5}$ s^{-1}, 35 % strain).

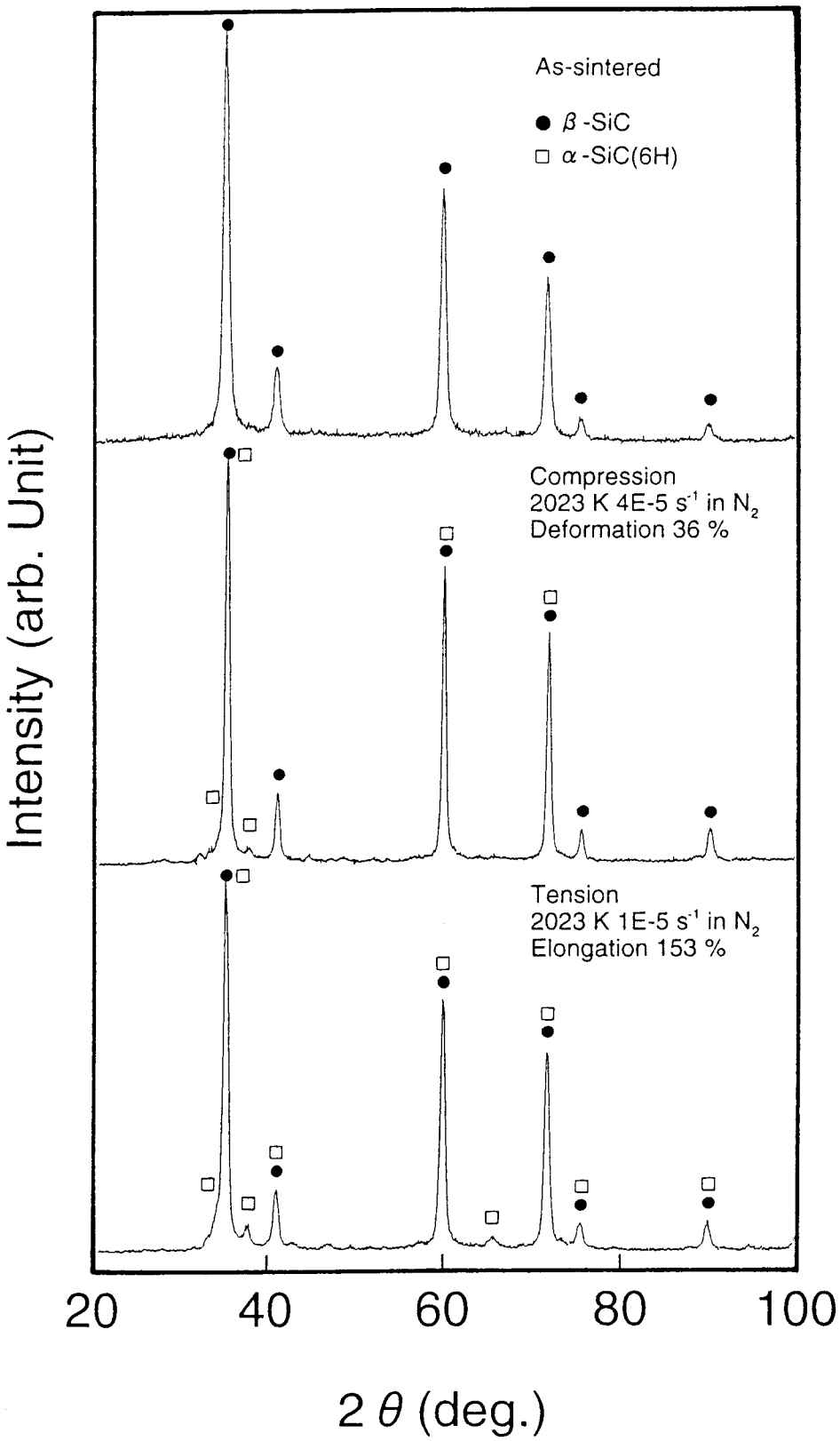

Fig. 11 X-ray results before and after deformation.

Grain boundary having thin amorphous film was observed in Fig. 5. The amorphous film at grain boundaries becomes a supercooled liquid at temperatures higher than the glass transition temperature. Therefore, grain-boundary phase contributes the deformation. The viscosity of glass phase increases by the addition of nitrogen. The increasing of viscosity causes the increasing of flow stress.

It was proposed that the mass transport was reduced by lattice strain arising from nitrogen incorporation into β-SiC [15]. Actually, Jun and co-workers reported that the sintering of SiC in N_2 showed lower densification rate, the suppression of phase transformation from β to α and grain growth in comparison with conventional Ar sintering[16].

Besides, only small amount of the cavitation was observed in 153 % tensiled specimen. Accordingly, the possibility of lowering deformation stress by cavitation damage was little.

Therefore, the flow stress and the deformation temperature of this material were concluded to be higher than that of β-SiC with the additions of Al_2O_3-Y_2O_3 due to the existence of nitrogen at grain boundaries, nitrogen incorporation into SiC grain and lower cavitation damage.

Judging from SEM observation of deformed specimens, strain hardening during deformation of this material is caused by the vaporization of grain-boundary phase and grain growth. Authors reported that the vaporization of grain-boundary phase caused rapid strain hardening in Al-doped β-SiC [17].

XRD result showed that the phase transformation from β to α after compression and tension tests were about 1 % and 20 %, respectively. The testing time of tension test was about 17 times longer than that of compression test. Moreover, the specimen annealed for the same time corresponded to the tension test at the same temperature showed about 15 %

phase transformation. Therefore, the effect of strain for phase transformation is a little.

Dislocation in SiC grains was slightly detected in compressed specimen. If the dislocation contribute the deformation, stress exponent should be between 3 and 5. However, stress exponents in compressive deformation were ranging from 1.7 to 2.1. Therefore, critical deformation mechanism is not dislocation movement. The inverse of grain size exponent was estimated by analyzing hardening in stress-strain curves assuming that the hardening occurred due to grain growth. The calculated value was 2.2 in compression test. This value does not have enough accuracy because we ignored the vaporization of grain-boundary phase during deformation. However, deformation behavior of this material was analogous to the superplastic metals ($n = 2$, $p = 2$).

Most of residual grain-boundary phase after tensile deformation existed at the triple points in Fig. 8. It suggested that grain-boundary phase was squeezed out by the tensile deformation and collected at the triple points at elevated temperature. Authors observed that the directly bonded two-grain junctions which grain-boundary phase was squeezed out and the tripe points which grain-boundary phase was collected in liquid-phase sintered β-SiC with the additions of Al_2O_3-Y_2O_3-CaO after superplastic compressive deformation[4, 18].

Moreover, the contribution of grain-boundary sliding to the total strain was calculated about 76 % in 153 % tensile deformed specimen. Therefore, critical deformation mechanism in this material is thought to be grain-boundary sliding.

5. Conclusion

Compression and tension tests of liquid-phase sintered β-SiC with the additions of 5.022 wt% Al_2O_3, 3.321 wt% Y_2O_3 and 0.657 wt% AlN at constant crosshead speeds were performed

by the universal testing machine at the initial strain rates of 1 X 10^{-4} s^{-1} to 5 X 10^{-6} s^{-1} in the temperature ranging from 1973 K to 2048 K in N_2. The results were as follows:

Compression test

(1) Stress exponents were from 1.7 to 2.1.

(2) Apparent activation energy was 776 KJ/mol. This value was between activation energy of lattice diffusion of Si and C, and that of grain-boundary diffusion of C.

(3) Phase transformation from β to α and dislocation in SiC grains were slightly observed. The anisotropy of grain growth was observed. The equiaxed grains were elongated in the perpendicular direction of compressive axis.

(4) The crystallization of grain-boundary phase was not observed even after compressive deformation. Some parts of grain-boundary phase was squeezed out or vaporized during compressive deformation.

Tension test

(1) Superplastic deformation of 170 % was achieved at the initial strain rate of 2 X 10^{-5} s^{-1} at 2048 K.

(2) Phase transformation from β to α about 20 % and the anisotropy of grain growth were observed in 153 % deformed specimen at 2048 K. The equiaxed grains were elongated in the direction of tensile axis.

(3) Much of grain-boundary phase was vaporized during tension test. Most of residual grain-boundary phase existed at the triple points.

The above suggested that critical deformation mechanism was grain-boundary sliding.

6. References

1. F. Wakai, S. Sakaguchi and Y. Matsuno, "Superplasticity of Yttria-Stabilized Tetragonal Zirconia Polycrystals," Adv. Ceram. Soc., **1** [3] 259-266 (1986).
2. Y. Shinoda, T. Nagano, H. Gu and F. Wakai, "Superplasticity of Silicon Carbide," J. Am. Ceram. Soc., in press.
3. M. Mitomo, Y-W. Kim and H. Hirotsuru, "Fabrication of Silicon Carbide Nanoceramics," J. Mater. Res., **11** [4] (1996) 1601-04.
4. T. Nagano, S. Honda, F. Wakai, and M. Mitomo, "Deformation of Liquid-Phase Sintered Silicon Carbide at Elevated Temperature," in Pro. of 6th Int'l Symp. on Ceramic Materials and Components for Engines, Ed. by K. Niihara, S. Hirano, S. Kanzaki, K. Komeya, K. Morinaga, (Japan Fine Ceramics Association, Tokyo, 1998) pp.707-712.
5. T. Nagano, H. Gu, Y. Shinoda, M. Mitomo and F. Wakai, "Tensile Ductility of Liquid-Phase Sintered β-Silicon Carbide at elevated Temperature," Ceramics: Getting into The 2000's, Part D, Edited by P. Vincenzini, (Techna, Faenza, 1999) pp.25-32.
6. T. Nagano, H. Gu, Y. Shinoda, G.D. Zhan, M. Mitomo and F. Wakai, "Tensile Ductility of Liquid-Phase Sintered β-Silicon Carbide at elevated Temperature," in Pro. of Towards Innovation of Superplasticity II," Ed. by T. Sakuma, T. Aizawa and K. Higashi, (Trans Tech Publications, Totton, 1999) pp. 507-512.
7. T. Nagano, K. Kaneko, G.D. Zhan and M. Mitomo, "The Effect of Atmosphere on Weight-loss of Sintered Silicon Carbide during Heat Treatment," Submitted to J. Am. Ceram. Soc..
8. T. Nagano, H. Gu, G.D. Zhan, and M. Mitomo, "Effect of Dynamic Microstructural Change for Tensile Deformation Behavior of Liquid-Phase Sintered β-Silicon Carbide with The Additions of Al_2O_3-Y_2O_3-CaO," Submitted to J. Am. Ceram. Soc..
9. H-W. Jun, H-W. Lee, G-H. Kim, H. Song, and B-H. Kim, "Effect of Sintering Atmosphere on The Microstructure Evolution and Mechanical Properties of Silicon Carbide Ceramics," Ceram. Eng. Sci. Proc., **18** [4] (1997) 487-504.
10. Y-W. Kim and M. Mitomo, "Fine-Grained Silicon Carbide Ceramics with Oxynitride Glass," J. Am. Ceram. Soc., in Press.
11. H. Tanaka and N. Iyi, "Simple Calculation of SiC Polytype Contents from Powder X-Ray Diffraction Peaks," J. Ceram. Soc. Jpn., **101** [11] (1993) 1313-1314.
12. A. Mukherjee, J.E. Bird and J.E. Dorn, "Experimental Correlations for High Temperature Creep," Trans. ASM **62** [1] (1969) 155-179.
13. M.H. Hon and R.F. Davis, "Self-diffusion of ^{14}C in Polycrystalline β-SiC," J. Mater. Sci., **14** [10] (1979) 2411-2421.

14. M.H. Hon, R.F. Davis and D.E. Newberry, "Self-diffusion of ^{30}Si in Polycrystalline β-SiC," J. Mater. Sci., **15** [8] (1980) 2073-2080.

15. W-S. Seo, C-H. Pai, K. Koumoto and H. Yanagida, "Microstructure Development and Stacking Fault Annihilation in β-SiC Powder Compact," J. Ceram. Soc. Japan, **99** [6] (1991) 443-447.

16. H-W. Jun, H-W. Lee, G-H. Kim, H-S. Song, and B-H. Kim, "Effect of Sintering Atmosphere on The Microstructure Evolution and Mechanical Properties of Silicon Carbide Ceramics," Ceramic Engineering & Science Proceedings, **18** [4] (1997) 487-504.

17. T. Nagano, K. Kaneko and H. Kodama, "Tensile Ductility of Al-Doped β-Silicon Carbide at Elevated Temperature," in Pro. of The Third Pacific Rim International Conference on Advanced Materials and Processing (PRICM3), Ed. by M.A. Imam, R. DeNale, S. Hanada, Z. Zhong and D.N. Lee, (The Minerals, Metals & Materials Society, Warrendale 1998) pp. 1897-1902.

18. T. Nagano, S. Honda, F. Wakai and M. Mitomo, "Compressive Deformation of Liquid-Phase Sintered Silicon Carbide at Elevated Temperature," Superplasticity & Superplastic Forming 1998, Edited by A.K. Ghosh and T.R. Bieler, (The Minerals, Metals & Materials Society, Warrendale, 1998) pp.247-256.